Final report

Marshall Plan fellowship

Benthic foraminifera of Upper Paleocene to Eocene strata in the Zagros Basin: Implications for sea-level fluctuations, paleoclimate and paleoenvironments around the PETM interval"

Seyed Hamidreza Azami

University of Vienna, Department of Geodynamics and Sedimentology, Vienna, Austria

Supervisors:

Prof Michael Wagreich

University of Vienna, Department of Geodynamics and Sedimentology

Prof R. Mark Leckie

University of Massachusetts-Amherst, Amherst, Department of Geosciences, Massachusetts, USA

Prof James Zachos

Department of Earth and Planetary Sciences, University of California at Santa Cruz,

Santa Cruz, California, USA

Abstract

This project introduced the subject of palaeoclimate and palaeoenvironmental research on fossil foraminifera related to finishing my PhD work as ongoing at the University of Vienna, Faculty of Earth Sciences, Geography and Astronomy, Department of Geodynamics and Sedimentology. My PhD project title is "Sedimentology and chemostratigraphy of Upper Paleocene to Eocene strata in the Zagros Basin: Implications for sea level fluctuations around the PETM interval". The project especially aims for a detailed record of environmental and climate change around the Paleocene-Eocene Thermal Maximum, an event that has been compared and can be correlated to today's rapid climate change.

In the course of the project several methods have been applied, including sedimentological field logging, measurements of carbonate content, organic carbon, carbon and oxygen isotopes, and trace element geochemistry. Biostratigraphy by calcareous nannofossil was used to constrain ages and sedimentation rates. The Paleocene-Eocene Thermal Maximum (PETM interval) could be identified by various proxies.

The detailed study of the benthic foraminiferal turnover and extinction event integrated with geochemical data can infer palaeoclimate evolution and paleoenvironmental consequences of the PETM. The Benthic Foraminiferal Extinction Event (BEE) was identified by the disappearance of several taxa of the DWAF (Deep Water Agglutinated Foraminifera) group, the last occurrence of Paleocene species and the first appearance of Eocene species. Some opportunistic taxa like *Bulimina*, *Tappanina* and *Quadrimorphina* are present in the studied section.

On the other hand, exploration of the past greenhouse events in ever increasing detail allow us to predict the effects of the warming of today's climate, caused by anthropogenic emission of CO_2 and its potential consequences for the biosphere.

Introduction

The Paleogene System records the transition from the major greenhouse climate phase of the Cretaceous to cooler climates and the onset of large ice sheets (Hay et al., 2004). This general climate evolution was punctuated by short-lived climate events termed hyperthermals (Abels et al., 2012; Zachos et al., 2008) such as the Paleocene-Eocene Thermal Maximum (PETM). The PETM constitutes one of the most abrupt and short-lived global warming events of the past 100 million years (Bains et al., 1999; Zachos et al., 2008). The PETM event was associated with a severe shoaling of the ocean calcite compensation depth and with a pronounced negative carbon isotope excursion recorded in carbonate and organic materials, reflecting a massive release of 13C-depleted carbon and widespread dissolution of seafloor carbonates (Zachos et al., 2003, 2005). The PETM with abrupt warming of around 10.000 years and other hyperthermals during the Paleogene serve as analogues of the recent anthropogenically-induced climate warming and associated global change (e.g. Bowen and Zachos, 2010). High-resolution stratigraphic correlation and a stable Paleogene time scale are thus critical for evaluation of rates of past global change to relate to recent global warming in the Anthropocene (Waters et al., 2017). The PETM event, more exactly the base of the CIE as the initiation of basal Eocene, has been used to define the base of the Ypresian Stage (early Eocene), and thus the base of the Eocene Series, with the Global Boundary Stratotype Section and Point (GSSP) "golden spike" at Dababiya, Egypt (Aubry et al., 2007). Various event scenarios were put forward for the PETM and other Paleogene hyperthermals (e.g. Pagani et al., 2006; Zachos et al., 2005) including light 13C from dissociation of methane hydrates (Dickens et al., 1997) and/or thermal combustion or oxidation of sedimentary organic matter (Svenson et al., 2004). The following early to midEocene time interval indicates a longer-term climate warming trend (e.g. Kelly et al., 2005) to the Early and

Middle Eocene Climatic Optimum (EECO/MECO) punctuated by short-term hyperthermal events, with astrochronological dating and timing of events in progress (Gradstein et al., 2012; Westerhold et al., 2012, 2017).

The early Paleogene was a climatically dynamic period with relatively rapid global warming events, called hyperthermals, superimposed on a warm background greenhouse climate. The best known and most extreme hyperthermal is the Paleocene–Eocene Thermal Maximum (PETM; Kennett and Stott, 1991; Thomas and Shackleton, 1996; Zachos et al., 2008), characterized by worldwide 5–8°C warming of Earth's surface as well as the deep oceans (McInerney and Wing, 2011; Dunkley Jones et al., 2013). The transition to this event has been estimated to have occurred within a few thousand years, the source and trigger of which still remains unknown although several hypotheses are currently debated (e.g., Dickens et al., 1997; Kent et al., 2003; Svensen et al., 2004; Higgins and Schrag, 2006; DeConto et al., 2012; Hönish et al., 2012; Dunkley Jones et al., 2013).

As well as the widespread geochemical anomalies such as the 2–3 ‰ negative $\delta^{13}C$ excursion in both marine and terrestrial environments (e.g., Kennett and Stott 1991; Thomas and Shackleton 1996; Zachos et al. 2001), the severe climatic perturbations of the PETM profoundly affected terrestrial and marine ecosystems, triggering faunal and floral radiations and migrations (e.g., Kelly et al., 1996; Bralower, 2002; Gingerich, 2003; Wing et al., 2005; Jaramillo et al., 2010; McInerney and Wing, 2011) including the most severe extinction of deep-sea benthic foraminifera recorded during the Cenozoic (Thomas, 1989, 1998, 2007; Kennett and Stott, 1991; Thomas and Shackleton, 1996; Alegret et al., 2009a, b; 2010; Giusberti et al., 2016). The benthic foraminifera extinction event (BEE) was rapid (<10 kyr; Thomas, 1989, 2003, 2007) and wiped out the Cretaceous bathyal and abyssal "Velasco-type fauna" (Berggren and Aubert, 1975;

Tjalsma and Lohmann, 1983; Thomas, 1998, 2007). The event was less severe in shelf environments (Gibson et al., 1993; Speijer et al., 2012; Stassen et al., 2015).

The cause of this global extinction is still under debate, because neither anoxia nor higher or lower productivity nor carbonate dissolution occurred globally at bathyal to abyssal depths in the deep sea, the largest habitat on Earth (e.g., Thomas, 2003, 2007; Alegret et al., 2010), and benthic foraminifera propagules are efficiently dispersed (Alve and Goldstein, 2003). The link between the environmental changes during the PETM and the benthic foraminiferal extinction event thus remains poorly understood. A common obstacle to perform detailed high-resolution studies of the PETM in deep-sea sediments is the fact that many records are condensed or discontinuous due to dissolution, especially across the few thousand years (Zeebe et al., 2014) of the onset of the carbon isotope excursion. The Paryab section represents an outstanding exception in that the section contains an expanded deep-sea record of the PETM, which has been studied because of its continuity and cyclostratigraphy. The cyclostratigraphic part is already published by Azami et al. (2018). Given the limited number globally of complete and expanded deep-sea PETM sections, the Paryab section represents an invaluable opportunity to investigate the environmental impacts of the PETM and repercussions on deep-sea benthic foraminifera.

Benthic foraminifera are very useful tools for palaeoenvironmental reconstructions because they have morphological diversity, narrow ecological tolerance, high abundance in marine sediments and good preservation potential (Friedrich, 2010). Benthic biota provides essential information on sea-level fluctuation, bottom water oxygenation and organic fluxes to the seafloor at the time of deposition (Jorissen et al., 1995; Van der Zwaan et al., 1999; Leckie and Olson, 2003).

Therefore, the detailed study of the benthic foraminiferal turnover and extinction event integrated with geochemical data can infer paleoenvironmental consequences of the PETM. On the other

hand, exploration of the past greenhouse events in ever increasing detail allow us to predict the effects of the warming of today's climate, caused by intense anthropogenic emission of CO_2 and its potential consequences for the oceans and the biosphere.

Geological Setting

Tthe Zagros Mountains are tectonically a part of the Alpine –Himalayan mountain belt, and formed after convergence between Eurasia and Gondwana, followed by collision of the Eurasian and African-Arabian plates and, finally, the closure of the Neo-Tethys Ocean in southwest Iran (e.g. Sengör, 1990). The Zagros Basin is the second largest basin in the Middle East with an area of about 553,000 km2, which extends from Turkey, northeastern Syria and northeaster Iraq throughout northwestern to southeastern Iran, forming nowadays the Zagros fold–thrust belt. The basin resulted from the continental collision between the Arabian margin and the Eurasian plate (e.g. Barbarian and King, 1981; Falcon, 1961) after Neo-Tethys subduction to the north, with the study area situated at the active margin during Late Cretaceous to Paleogene times (e.g. Saura et al., 2011). During the Paleocene to Eocene, the Zagros Basin was situated on the eastern continental margin of the Tethys and provides a Cenozoic carbonate platform margin and a deeper-water pelagic depositional area characterized by alternating carbonates and fine-grained siliciclastics (Sengör, 1990). The cyclic limestone-marl successions of the Paleocene–lower Eocene Pabdeh Formation were deposited in a deeper-water bathyal marine environment in the (closing) oceanic area of the NeoTethys, and consist of deep-water pelagic to hemipelagic shale, marl(stone) and limestone. Above this shaly lower part a cyclic limestone-marl succession follows, overlain by limestones of the Asmari Formation.

The lithology, sedimentology, calcareous nannofossil-stratigraphy and carbon-oxygen isotopes have been already studied for the Pabdeh Formation in the Paryab section, including higher resolution for the PETM interval. A total of 394 samples have been taken from the predominantly 171-m thick including the shaly lower part and marly (limestone-rich) upper part of the Pabdeh Formation in the section at the village of Paryab, NW Iran (N 33°15'14", E 46°37'3.2"). However, due to outcrop conditions, sampling intervals varied within the section, above 2 m distance in the lower shaly section part up to 60 m, and a more denser sampling interval of below 50 cm in the middle part of the section including the shaly PETM. The upper part of the section, displaying marl-limestone cycles from 116 m onwards, was sampled bed-by bed for every marl and limestone bed, resulting in a mean sampling distance of 40 cm. The cyclic limestone-marl successions of the Paleocene–lower Eocene Pabdeh Formation (Fig. 1) were deposited in the (closing) oceanic area of the Neo-Tethys, and consist of deep-water pelagic to hemipelagic shale, marl(stone) and limestone.

Fig. 1: Pabdeh Formation, cyclic (limestone)-marl successions of the Lower Eocene.

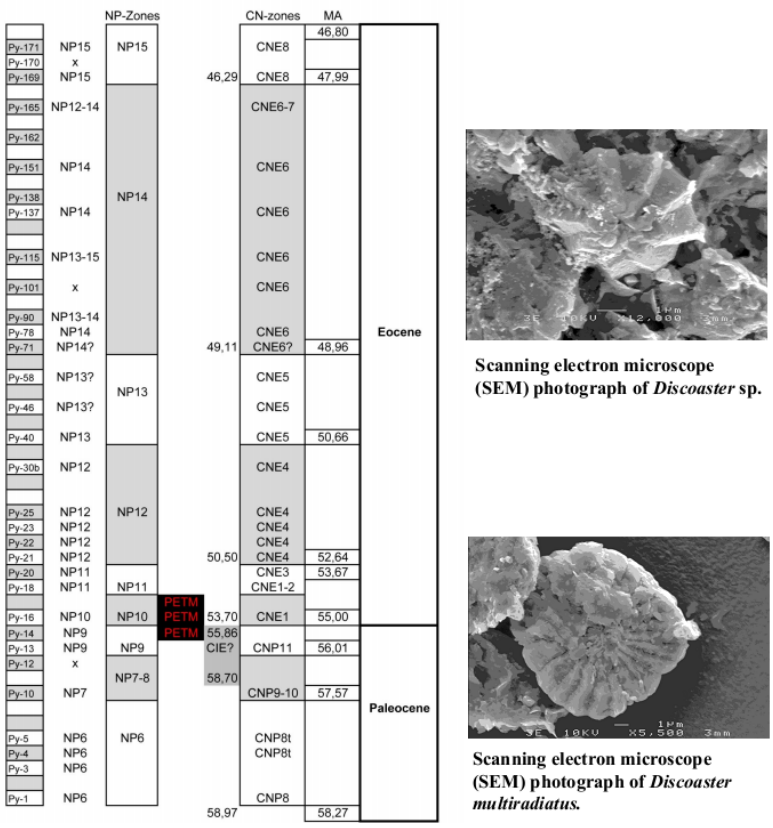

Fig. 2: Nannofossil overview stratigraphy of the Paleocene-Eocene interval in the Pabdeh Formation, PETM interval marked in black. The PETM is characterized by specific nannofossil and foraminiferal assemblages, and a negative carbon isotope excursion. Higher up-section, *Sphenolithus moriformis* and *Discoaster diastypus* appear, and $\delta^{13}C$ values increase again.

Material and methods

The special procedure for 39 foraminifera sample preparation was performed during the stay in USA at the micropaleontology lab of Prof. Leckie at UMass:

1. Weighed sediment was put into a >63 um sieve (a small pea-sized amount of sediment is kept in case anyone wants to do smear slide analyses, etc. in the future).

2. Sediment was washed with warm tap water until there was no more clay coming out of the sediment.

3. The sieved sediment was gently washed into a petri dish (or other small dish or glassware).

4. Samples were dried in the oven overnight or until dry at ~50 degrees Celsius (Any warmer temperature may affect the calcite for geochemical analyses later).

5. When sieved sediment was dry, it was placed into a labeled jar for further analyses.

Between washing samples, care was taken to thoroughly rinse the sieve. Blue liquid (Methylene Blue) was added to identify any contamination in the next samples.

Method for use UMass Freeze dryer:

- With the machine vacuum pump off, pick up giant stainless-steel container and remove/soak up excess water that has accumulated
- Insert plug into hose behind machine (otherwise device won't be sealed for a vacuum when machine turned on)
- Load samples
    - Two ways to do so: use external canisters
    - Load into giant stainless-steel container

- If you opt for this, put sample on stackable carousel, and plug that to the warmer; it well help remove moisture to decrease more efficiently otherwise it could be a lot longer

- Press refrigerate and wait for the temperature to decrease to -46-50C
- Press vacuum
- Pressure will start off high, around 500, record value and leave
- If you hear a weird noise, it most likely meant that likely means that is not a tight seal
    - Check to make sure hose is plugged
    - Check other valves to make sure they are all turned to the off position
        - When the vacuum has reached low values, around 70, and its been holding that value for a day or so, then you can assume all moisture has been removed
        - Press vacuum to turn off pump, and slowly open one of the valves
        - Once everything has reached equilibrium, you can remove canister, or open stainless-steel container (depending on which way you loaded samples)
        - If you are loading more sample, add them now, and press pump once you are finished, otherwise:
        - Turn off refrigerator
        - Remove plug from back of machine to drain excess water

The aims of this project were to accomplish the combination of detailed benthic foraminiferal analyses on sampled and processed rock material as follows:

Quantitative foraminifera evaluation methods

Abundance and diversity

The oxygen content of bottom water and nutrient availability are the most important factors that influence benthic foraminiferal assemblages and control their abundance and diversity (Jorissen et al., 1995; Van der Zwaan et al., 1999). In the low oxygen sediments, benthic foraminifera number and diversity generally decreases due to oxygen consumption and benthic foraminifera become absent in highly oxygen-depleted sediments (Friedrich et al., 2005, 2006). The absolute abundance (Ng^{-1}: number of benthic foraminifera per gram of bulk dried sediment) for both the ≥63 and ≥500 μm fractions and faunal diversity indices (species diversity and Fisherα) coeval with other factors allow us to determine the oxygen contents and productivity in the basin.

Benthic foraminiferal morphogroups

In the absence of single species isotope data, benthic foraminiferal morphogroups provides a useful basis for environmental interpretation. Kaminski and Gradstein (2005) presented a model for agglutinated foraminiferal morphogroups. In this model organic matter arriving at the sea floor will be first scavenged by the tubular (M1morphotype) agglutinated species that extend their pseudopodia to capture food from the water column. The organic matter that arrives on the sediment surface will be then consumed by epifauna or shallow infauna (M2, M3a, M3b and M4a morphotypes) that utilize various feeding strategies. The remaining organic matter will arrive into the sediment by bioturbation or after burial, and be made available to the deep infauna taxa (M4b morphotypes) which using their elongate shapes easily move into the sediments. Therefore, higher organic matter influx into the basin sustain high populations of the deep infauna morphogroup (M4b), which is situated at the end of the food chain. Also, due to reduction of oxygen content in the pores of sediments with an increase of depth, deep infauna morphogroups are interpreted to be resistant to oxygen deficiency.

Response of calcareous benthic foraminifera to variations of organic matter and oxygen level is similar to agglutinated forms; deep infauna morphogroups dominate when organic matter increases and oxygen level decreases, however calcium carbonate dissolution also plays an important role in calcareous benthic foraminifera assemblages (Koutsoukos et al., 1990; Frenzel, 2000; Cetean et al., 2011).

Quantitative studies of benthic foraminifera will be based on representative splits (using a modified Otto microsplitter) of approximately 300 specimens larger than 63 μm.

Benthic formaniferal Oxygen Index (BFOI)

The BFOI was developed by Kaiho (1994) using various morphologic and taxonomic parameters. Calcareous benthic foraminifera are divided into dysoxic (0.1–0.3 mL/L), suboxic (0.3 –1.2 mL/L), and oxic (N 1.2 mL/L) indicators on the basis of relations between specific morphologic characters (or species composition) and oxygen levels and calcareous benthic foraminiferal microhabitat. Late Paleocene – early Eocene oxic, suboxic, and dysoxic indicators encountered in this study are as follows: Oxic indicators (≥ 350 μ m, thick wall, epifaunal in high oxygen bottom water) consist of *Nuttallides truempyi*, *Stensioeina beccariiformis*, and *Conorbinoides hillebrandti*. Dysoxic indicators (thin wall, elongate, flattened, infaunal in high oxygen bottom water) consist of 1) non-ornamented buliminids, 2) nonornamented small *Nodosaria*, *Dentalina*, and *Stilostomella*, 3) *Bolivina* and *Coryphostoma* (flattened), 4) *Abysssamina* and *Quadrimorphina* (small, thin wall). The other calcareous benthic foraminifera are suboxic including small specimens of oxic species (<350 μm) (Kaiho et al., 2006).

Dissolution indices

A) Coarse Size Fraction

Carbonate dissolution within the lysocline commonly leads to fragmentation of foraminifer tests, which decreases the coarse size fraction of bulk sediment (Berger et al., 1982; Broecker and Clark, 1999; Hancock and Dickens, 2005). After wet sieving, the coarse (>63 μm) component will be dried and weighed. This mass divided by bulk sample mass rendered the coarse (>63 μm) size fraction.

B) Benthic Abundance

The relative abundance of benthic foraminifers (BENTH) is expressed as a ratio of benthic foraminifers to the sum of benthic and planktonic foraminifers. Benthic foraminifers are less susceptible to dissolution than planktonic foraminifers because the latter typically have porous chamber walls designed to maintain buoyancy in surface waters. Thus, the relative abundance of benthic foraminifers may serve as an index for carbonate dissolution at deep-water sites (Schlanger and Douglas, 1973; Thunell, 1976; Hancock and Dickens, 2005).

Palnktic/benthic ratio also can be used to determine water depth (Van der Zwaan, 1999; Van Hinsbergen et al., 2005). In ideal open shelf environments with normal changes in the oceanographic variables, % benthic decrease in deeper water probably because of less food delivery to the sea floor (e.g., Jorissen et al., 1995; Leckie and Olson, 2003).

C) Foraminiferal Fragmentation

A foraminiferal fragment (F) is defined as a test portion less than two-thirds of its original size. The fragmentation index (FRAG) for each sample was calculated according to the following equation (Williams et al., 1985; Malmgren, 1987):

FRAG = (F/8)/[(F/8) + whole planktonic foraminifers]

The number of fragments is divided by 8 because, on average, one foraminifer breaks into this number of fragments and it is the proportion of fragmented foraminifers, rather than the number of fragments themselves, that has a near-linear relationship with dissolution (Le and Shackleton, 1992). Benthic foraminifers are not included in the whole foraminifer count as their tests are more resistant to dissolution than planktonic foraminifers.

Nannofossil biostratigraphy

100 samples were processed using the standard smear-slide technique to prepare nannofossil samples for light microscopy (Bown, 1998). Small amount of decanted in 50 ml distilled water, then placed for 30 s in an ultrasonic bath. Next, the materials were to be settled for 1 min. After pouring out the upper solution and settling for 1 hour, the supernatant was poured off and the residue was diluted with distilled water and used for slide. Small amount of material scraped on to cover slip, drop of water added, mixed and smeared using a toothpick, dried on a hotplate, and the cover slip was attached with Canada balsam to the slide and also one drop was dried on the filter for SEM examination. Biostratigraphic age determination is based on qualitative examination using 100x oil immersion light microscope. Standard nannofossil zonations of Martini (1971) and Agnini et al. (2014) are applied.

Carbonate contents and total organic carbon

the carbonate content was measured by Müller-Gastner-Bomb devices (Müller and Gastner 1971) using diluted hydrochlorid acid on 273 samples. An error range for individual measurements of 1% CaCO3 is reported based on frequently run calibration samples. The mean sampling distance of around 63 cm corresponds to a time resolution of one sample each c. 37 ka.

Whole rock carbonate stable carbon isotopes

This study includes $\delta^{13}C$ data for the PETM interval of the Pabdeh Formation of the study area (a carbon and oxygen isotope curve of the whole section is in preparation). 44 powdered samples were analyzed for stable carbon and oxygen isotopes using a Thermo Fisher DeltaPlusXL mass spectrometer equipped with a GasBench II following the procedure of Spötl and Vennemann (2003) at the University of Innsbruck. The δ13C values are corrected according to the NBS19 standard and reported in per mil (‰) relative to the Vienna-PeeDee Belemnite (V-PDB) standard; analytical precision was at 0.05% for $\delta^{13}C$.

Results

Calcareous Nannofossil biostratigraphy

Nannofossil biostratigraphy indicates standard zones NP6 to NP14 of Martini (1971) and CNP8 to CNE8 of Agnini et al. (2014), respectively, for the studied section of the Pabdeh Formation at Paryab. Biostratigraphic age determination is based on calcareous nannoplankton using smear slides and 100x oil immersion light polarization microscope. Nannofossil biostratigraphy indicates standard zones CNP8 to CNE8, respectively, for the whole section of the Pabdeh Formation at Paryab. The PETM interval is indicated by several distinct nannofossil taxa starting at 69.1 m: *Rhomboaster* spp. (mainly *Rhomboaster cuspis*), *Discoaster araneus*, and the disappearance of the *Fasciculithus richardii* group (Fig. 3). The section includes the following identified nannofossil zones:

Nannofossil Standard Zone CNP8 - NP6

The interval from the base of the section (0m) to 47.5 m records nannofossil standard zone CNP8 (Agnini et al., 2014: *Heliolithus cantabriae* Zone) and NP6 (Martini, 1971; Perch-Nielsen, 1985; *Heliolithus kleinpellii* Zone). *Heliolithus kleinpellii* is present throughout that interval in the Paryab section, together with various *Fasciculithus* (*F. tympaniformis, F.* cf. *bitectus, F. ulii, F. janii*) and rare *Sphenolithus anarrhopus*. The presence of *Heliolithus kleinpellii* indicates NP6 of Martini (1971). Although different morphotypes of *H. kleinpellii* are present, no typical *Heliolithus cantabriae* could be found, therefore, the middle to upper part of CNP8 is indicated according to Agnini et al. (2014).

The assemblages are predominated by common *Coccolithus pelagicus, Sphenolithus* spp. (mostly *S. primus*), *Cruciplacolithus* ssp. (*C. frequens, C.* cf. *asymetricus, C. intermedius*) and few *Toweius eminens, T. pertusus, Ericsonia subpertusa* and *Operculodinella* sp. Rare *Neochiastozygus* (*N. distentus, N. saepes*), *Chiasmolithus* (*C. consuetus*), *Ellipsolithus macellus, Prinsius* sp., *Zygodiscus* ssp. are present.

Reworked specimen from Upper Cretaceous (e.g. *Lucianorhabdus cayeuxii, Arkhangelskiella cymbiformis, Cribrosphaerella ehrenbergii*) and Lower Paleocene (e.g. *Placozygus fibuliformis*) make up a few percent of the assemblages.

Nannofossil Standard Zone CNP9/10 - NP7/8

The interval from 47.5 m to 62.5 m is assigned to nannofossil standard zones NP7/8 (Martini, 1971; Perch-Nielsen, 1985: *Discoaster mohleri* Zone and *Discoaster nobilis* Zone) and CNP9/10 (Agnini et al., 2014: *Discoaster mohleri* Zone and *Discoaster backmanii* Zone). *Discoaster mohleri* is consistently present in this interval. and *D. nobilis* occurs rarely. *Coccolithus pelagicus* is again abundant, other common genera include *Fasciculithus, Sphenolithus, Toweius*. Further evolved *Fasciculithus* like *F. clinatus* can be found.

Within the rather low resolution study of this section interval no distinct base for *Discoaster nobilis* (very rare from 62.0 m onwards) or *Discoaster backmanii* (not identified unambiguously) could be found, therefore we join the two zones into one combined nannofossil zone. *Heliolithus kleinpellii* has its top within this zone at 50.0 m.

Nannofossil Standard Zone CNP11 - NP9a

The interval from 62.5 m to 67.9 m is assigned to nannofossil standard zones NP9 (Martini, 1971; Perch-Nielsen, 1985: *Discoaster multiradiatus* Zone) and CNP11 (Agnini et al., 2014: *Discoaster multiradiatus/Fasciculithus richardii* Concurrent Range Zone). *Discoaster multiradiatus* appears at 62.5 m. Nannofossil standard zone NP9 was further subdivided into 2 subzones (e.g. Aubry et al., 2007), with NP9a defined by the base of *Discoaster multiradiatus*, and the base of *Rhomboaster* spp. defining the base of NP9b; thus, in the zonal scheme of Aubry et al. (2007) this interval can be assigned to subzone NP9a.

Nannofossil Standard Zone CNE1 - NP9b

Nannofossil zone CNE1 (Agnini et al., 2014: *Fasciculithus tympaniformis* Zone) or subzone NP9b ranges from 67.9 to 69.1 m in the Paryab section. The *Fasciculithus richardii* group disappears at 67.9 m. The first morphotypes of *Tribrachiatus/Rhomboaster* appear at 69.1 m, *Rhomboaster* spp., mainly *Rhomboaster cuspis*. *Discoaster araneus* also has its base in this interval as well as *Spenolithus* cf. *moriformis*. The disappearance of common *Fasciculithus tympaniformis* at 69.1 m is coeval with the base of *Rhomboaster* spp.

Nannofossil Standard Zone CNE2 - NP10

The interval from 69.1 m to 76.2 m is assigned to nannofossil standard zone CNE2 (Agnini et al., 2014: *Toweius eminens* Partial Range Zone). This correlates to the lower part of NP10 (Martini, 1971; Perch-Nielsen, 1985: *Tribrachiatus contortus* Zone), corresponding most probably to NP10a of Aubry et al. (2007). Subzones NP10a, NP10b, NP10c, NP10d are defined by the

Tribrachiatus lineage of *T. bramlettei* - *T. digitalis* - *T. contortus* - *T. orthostylus* (Aubry et al., 2007). *Discoaster diastypus* appears at 73.2 m in this zone. The first *Tribrachiatus* in our study, *T. contortus*, appears at 76.2 m and may thus define the base of NP10d of Aubry et al. (2007).

Nannofossil Standard Zone CNE3 - NP11

The interval from 76.2 m to 87.6 m ranges into nannofossil standard zone CNE3 (Agnini et al., 2014: *Tribrachiatus orthostylus* Zone). This correlates to the uppermost part of NP10 (NP10d) and the whole NP11 zone (*Discoaster binodosus* Zone) of Martini (1971). The first *Tribrachiatus orthostylus* occurs rarely at 76.2 m, still together with *Rhomboaster cuspis*. *Rhomboaster bramletteii* has its first sporadic occurrence at 78.6 m, *Discoaster barbadiensis* at 79.2 m. *Tribrachiatus digitalis* and *Coccolithus bownii* start at 81.6 m, *Sphenolithus radians* and *Discoaster binodosus* start consistently at 82.6 m. The last occurrence of *Tribrachiatus contortus* at 83.6 m defines the top of NP10 which thus covers an interval up to 83.6 m; however, the range of *T. contortus* overlaps completely with (rare) *T. orthostylus*.

Nannofossil Standard Zone CNE4 - NP12

The interval from 87.6 m to 124.1 m is assigned to nannofossil standard zone CNE4 (Agnini et al., 2014: *Discoaster lodoensis/Tribrachiatus orthostylus* Concurrent Range Zone) and NP12 (*Tribrachiatus orthostylus* Zone) of Martini (1971). The first *Discoaster* sp. aff *D. lodoensis* (Fig. 4N) occurs at 87.6 m defining the base of CNE2 (base common *Discoaster lodoensis* of Agnini et al., 2014) and NP12; however, this species is rather rare throughout the section.

Common *Coccolithus pelagicus* and *Sphenolithus* spp. (mainly *S. radians*) characterize the assemblages, besides *Discoasters* (e.g. *D. barbadiensis, D. salisburgensis, D. mahmoudi*) *Toweius gammation*, and rare *Chiasmolithus* (*C.* cf. *californicus*).

Nannofossil Standard Zone CNE5 - NP13

Nannofossil zone CNE5 (Agnini et al., 2014: *Reticulofenestra dictyoda* Partial Range Zone) ranges from 119.6 m to 138.7 m, and correlates to NP13 (*Discoaster lodoensis* Zone). The last occurrence of *Tribrachiatus orthostylus* is at 119.6 m, *Discoaster lodoensis* is still rarely present. Besides *Discoaster* spp. (*D. salisburgensis, kuepperi, barbadiensis, lodoensis), Sphenolithus radians* dominates the assemblages, whereas *Coccolithus pelagicus* decreases.

Nannofossil Standard Zone CNE6 - NP14

The interval from 138.7 m 158.8 m is assigned to nannofossil standard zones CNE6 (Agnini et al., 2014: *Discoaster sublodoensis/Discoaster lodoensis* Concurrent Range Zone) and the lower part of NP14 (*Discoaster sublodoensis* Zone) of Martini (1971). The first five-rayed *Discoaster* cf. *sublodoensis* (Fig. 4O) occurs sporadically at 138.7 m together with *Discoaster lodoensis.* The top of *D. lodoensis* is around 158.8m.

Nannofossil Standard Zone CNE7 - NP14

The interval from 158.8 m to 172.0 m is assigned to nannofossil standard zones CNE7 (Agnini et al., 2014: *Discoaster barbadiensis* Partial Range Zone) and the middle part of NP14 (*Discoaster sublodoensis* Zone) of Martini (1971). The top of *D. lodoensis* is recorded at 158.8m, defining the base of CNE7.

Nannofossil Standard Zone CNE8 - NP14

The top of the Paryab section from 172.0 m to 172.4 m is assigned to nannofossil standard zone CNE8 (Agnini et al., 2014: *Nannotetrina cristata* Zone) and the uppermost part of NP14 (*Nannotetrina fulgens* Zone) of Martini (1971). *Nannotretina cristata* (Fig. 4P), the first *Nannotetrina* species recorded, occurs from 172 m onwards.

Blackites spp. (*Blackites spinosus, B. stylus*) and *Reticulofenestra* (mainly *R. dictyoda* and *R. bisecta*) are present. In addition, *Sphenolithus* spp. show an evolutionary step to forms that may lead to *Sphenolithus furcalithoides* higher up.

Table 1: Nannofossil biostratigraphy (CNE zones of Agnini et al., 2014), ages of bioevents in million years (Ma), meter in section, age durations of intervals, difference in section meter, and sediment accumulation rates in mm/ka.

		Ma	Meter		dMa	dMeter	mm/ka
Base and top of bioevents/zones							
B *Nannotetrina cristata*	CNE8	47,99	172,0		0,97	33,3	34,33
T *Discoaster lodoensis*	CNE7	48,37	158,8	158.8m			
B *Discoaster sublodoensis* (5-rayed)	CNE6	48,96	138,7		4,71	62,5	13,27
T *Tribrachiatus orthostylus*	CNE5	50,66	119,6				
B *Discoaster lodoensis*	CNE4	52,64	87,6	87.6m			
T *Tribrachiatus contortus*		53,49	83,6	83.6m			
B *Sphenolithus radians*		53,53	82,6	82.6m			
Tc *Discoaster multiradiatus*		53,58	80,2				
B *Tribrachiatus orthostylus*	CNE3	53,67	76,2	81.2m/76.2m	2,34	13,7	5,85
B *Tribrachiatus contortus*		54,00	76,2	76.2m			
B *Discoaster diastypus*		54,13	73,2	73.2m			
T *Fasciculithus tympaniformis*	CNE2	54,71	69,1				
B *Rhomboaster* spp.		54,99	69,1	69.1m			
T *Fasciculithus richardii* group	CNE1	55,00	67,9				
B *Discoaster multiradiatus*	CNP11	56,01	62,5				
B *Discoaster nobilis*		56,25	62,0	62.0m			
T *Heliolithus kleinpellii*		57,42	50,0	50.0m			
B *Discoaster mohleri*	CNP9	57,57	47,5	47.5m	0,70	47,5	67,86
B *Heliolithus kleinpellii*		58,03	5,0	5.0m			
B *Heliolithus cantabriae*	CNP8	58,27	0,0	0.0m?			

Cyclostratigraphic evaluation

The cyclostratigraphic analysis of Azami et al. (2018) found several significant spectral peaks above the 80% confidence interval and fulfilling significance criteria. Significant harmonics that clearly meet the requirements were identified at 36.12 m, 5.49 m, and 3.49 m and in the frequency band between 2.47 to 1.89 m. The evolution of significant harmonics visualized in the EHA (Azami et al., 2018: Fig. 7 and 8) shows two distinct harmonic frequencies that are present throughout almost the whole section. Seemingly continuous signals can be followed from 70 m at 0.1 cycles per/m to 140 m with at 0.07 cycles/m as well as and from 70 m with 0.18 cycles/m to 135 m with 0.35 cycles/m. Other signals visible in this analysis seem to be discontinuous and show a patchy distribution. The spectral resolution between 70 and 120 m suffers from an under sampled interval in the shales present in the older segments of the section. The resolution of the topmost intervals in the EHA shows several faint signals between 0.5 and 1.5 cycles /m (Azami et al., 2018: Figure 7).

The interval subject to cyclostratigraphic investigation was chosen by Azami et al. (2007) from the PETM interval to the top of the section, because of the relatively dense sample positions, the presence of a probably undisturbed succession between 69.1 and 172 m and the astronomically calibrated onset of the PETM at 55.93 Ma (Westerhold et al., 2012, 2017), that is evident in the lowermost segment of this interval. Despite a difference in lithological properties, data from shales and overlying limestone/marl rhythmites were not analyzed separately as sedimentation rates inferred from biostratigraphic data suggest an almost uniform sedimentation rate from 50 m onwards (Azami et al., 2018: Figure 5).

According to Azami et al. (2018) in the LOWSPEC analyses of the untuned record of the carbonate contents, the signal likely to represent the stable 405 ka cycle (Gradstein et al., 2012)

was identified. Also evident in the raw data are signals that might correspond to the long 2.4 Ma- and the short ~100 ka eccentricity cycle. Other shorter signals evident in the LOWSPEC analysis of carbonate content raw data are either discontinuous and cannot be attributed an astrochronomical target, or suffer from poor sample resolution (Azami et al., 2018).

Azami et al. (2018) tuned the carbonate contents signature to the theoretical 405 ka cycle (their Figure 8 and Table 2). Significant signals visible in spectral analyses of the tuned record include two short eccentricity terms of 100 and 90 ka durations and a 291 ka harmonic frequency that cannot be attributed an orbital target. The EHA of the tuned time series also shows evidence for prominent harmonic signals below the 405 ka frequency band that represent durations from 800 to 1900 ka. As these signals are not present in the robust LOWSPEC analyses, Azami et al. (2018) interpreted these signals as harmonic artefacts that originated from orbital tuning and represent multiples of harmonic frequencies. The tuned $\%CaCO_3$ sequence from the onset of the PETM at 69.1 m to the top of the Paryab section as reported by Azami et al. (2018) spans a total of 8.566 Ma and records twenty one 405 ka eccentricity cycles.

Azami et al. (2018) compared the duration of the orbitally tuned carbonate contents data to estimates for the Eocene nannofossil zonations (see Agnini et al., 2014): The base of the Lutetian and nannofossil zone CNE8 (Agnini et al., 2014) at 170 m can be dated with~47.45518 Ma. Agnini et al. (2014) give an age of 47.99 Ma for the base of this zone. Thus, the age estimate of Azami et al. (2018) for the base of CNE8 at the Paryab section was approximately one 405 ka eccentricity cycle off the calibrated age for this zone. The reasons for that could be flaws in their cyclostratigraphic model, gaps in the record at Paryab section or diachroneity of nannofossil markers. In addition, differences in the exact timing of the onset of the PETM are plausible, e.g.

Agnini et al. (2014) use a different age of 55.0 Ma for their base of the PETM CIE (and base of CNE1) than the tuned data by Westerhold et al. (2012, 2017).

The PETM interval

From 68.8 m to 69.1 m in the Paryab section, carbon isotope values fall from 1.68‰ to -0.23‰ (Fig. age-depth inset) depicting the beginning of the distinct negative carbon isotope excursion (CIE). This coincides in the same sample with the base of nannofossil zone CNE2 (Agnini et al., 2014: *Fasciculithus tympaniformis* Zone). The disappearance of the *Fasciculithus richardii* group appears 1.2m below this level, at 67.9 m. The first *Rhomboaster cuspis* and *Discoaster araneus* appear also at this level, as well as the disappearance of common *Fasciculithus tympaniformis*, attesting to the base of the PETM interval (Aubry et al., 2007).

Lithologically, there is no visible sign of changes in sedimentation as known from other sites, e.g. carbonate dissolution or black shale deposition. Carbonate contents fluctuate around the PETM interval from 47 to 72%, without a clear-cut regularity. Although the onset of the PETM-CIE can be defined precisely, the following interval does not show a typical PETM $\delta^{13}C$ excursion pattern, but fluctuations, followed by a longer term plateau phase upwards (Azami et al., 2018).

Assemblages at Paryab are typically Tethyan/low-latitude and of warm-water character, with lots of *Discoaster* and other warm-water species (e.g. Bown, 1998; Agnini et al., 2014). The nannoplankton assemblages allow the identification of the PETM interval due to the large turnover in assemblages at the base of the PETM interval (Aubry et al., 2007). This short-term marine warming was followed by a long-term cooling after the early-middle Eocene. Though thermal variation from warmer ocean waters during the PETM to the cooler ocean water

temperatures afterwards is likely to have decreased the effects of Milankovitch cyclicity on the sedimentation pattern, however, significant facies change from shales to shale-marl cycles can be identified in the section after the PETM interval, and may be regarded as an expression to higher productivity of calcareous plankton organisms in the aftermath of the event.

The base of the Ypresian

The Ypresian Stage comprises the lowermost stage of the Eocene, with the Paleocene/Eocene boundary at the base; therefore, the base of the Ypresian is equivalent to the base of the Eocene, and, consequently, relates to the lower Eocene. The classical stratotype is situated in western Belgium (Gradstein et al., 2012). The modern GSSP was defined in the Dababiya section near Luxor, Egypt (Aubry et al., 2007). The marker event chosen was the onset of the PETM CIE, i.e. the onset of the 2.5 to 4‰ negative carbon isotope excursion. Correlations to secondary marker include: (1) the lower to middle part of magnetochron C24r – at C24r.36, c. 1.4 Ma above the base of C24r, (2) a position within nannofossil zone NP9 marked by the occurrence of the *Rhomboaster-Discoaster araneus* assemblage (Aubry et al., 2007) or the CNET, the calcareous nannofossil excursion taxa (Agnini et al., 2014). The base of the Ypresian thus correlates to the top of the *Fasciculithus richardii* group, *the base of Rhomboaster* spp. and the subsequent top of *Fasciculithus tympaniformis*/spp. (Aubry et al., 2007; Agnini et al., 2014).

Planktonic foraminifera excursion taxa such as *Acarinina africana, A. sibaiyaensis* and *Morozovella allisonensis* have been identified at various sections including the GSSP in Egypt (Aubry et al., 2007). Benthic deep water taxa that became extinct are *Stensioeina beccariiformis, Angulogavelinella avnimelechi, Coryphostoma midwayensis, Aragonia velascoensis, A.*

ouzzanensis, Gavelinella hyphalus, G. rubiginosus, G. velascoensis, Neoflabellina jarvis and *N. semireticulata, Neoeponides hillebrandti, Osangularia velascoensis,* and *Pullenia coryelli*.

The age of the base of the Ypresian, and thus the onset of the PETM interval, is still in discussion. Gradstein et al. (2012) indicate a numerical age of 56.0 Ma or 55.96 Ma, with the base of *Rhomboaster* spp. at 55.96 Ma, whereas Agnini et al. (2014) give an age of 55.0 Ma for the top of the *Fasciculithus richardii* group, and 54.99 for the base of *Rhomboaster* spp. Westerhold et al. (2012, 2015, 2017) combining astrochronology and available geochronological data report most recently an age of the PETM base at 55.930 Ma (option 2 in Westerhold et al., 2012).

The studied section at Paryab provides a high resolution record around the onset of the PETM and thus the Thanetian/Ypresian and Paleocene/Eocene boundary. The base of the CIE is, however, not defined unambiguously – a first slight decrease of values start at 68.2 m (from 1.40 to 0.91‰) followed by a slight increase ($\delta^{13}C$ of 1.23 and 1.68‰) and a final abrupt decrease to -0.23‰ from 68.8 to 69.1 m. We take this level as the actual onset of the CIE, keeping in mind the small bias introduced by using the onset of a chemostratigraphic signal/peak - a small uncertainty in correlations due to sample spacing and analytical errors already noted by Aubry et al. (2007). At 69.1 m, as *Rhomboaster* spp. and other CNET taxa (Aubry et al., 2007; Agnini et al., 2014) occur. Applying the Laskar 2010 astrochronological solution and the tuned $\%CaCO_3$ record (Azami et al., 2018) we infer the Thanetian/Ypresian boundary at a precise position within the $Ec_{405}1$ cycle of Westerhold et al. (2017). However, using the Agnini et al. (2014) age of 55 Ma for the base of the Ypresian, this datum may already fall into $Ec_{405}3$, giving still a possible correlation uncertainty of 2 long eccentricity cycles (Azami et al., 2018).

Foraminifera

Foraminiferal assemblages through the section are characterized by a predominance of planktonic foraminifera, Benthic foraminifera count normally less than 10% of the assemblages. Detailed foraminifera evaluation around the PETM started at the University of Massachusetts Amherst, but is still in progress. However, the first results can be presented herein.

Planktonic foraminifera zones identified in the wider study area include the *Morozovella velascoensis* Zone (crossing the Thanetian-Ypresian boundary), defined by the LO (Last Occurrence) of *Globanomalina pseudomenardii* to the LO of *Morozovella velascoensis* or the FO of *Morozovella formosa*, the *Morozovella formosa* Zone, the base defined by FO of *Morozovella formosa*, and its top by the FO of *Morozovella aragonensis* (early Ypresian). Then follows the *Morozovella aragonensis/Morozovella subbotinae* Zone defined by FO of *Morozovella aragonensis* and the LO of *Morozovella subbotinae* (Ypresian).

The Benthic Foraminifera Extinction Event (BEE) was identified in the samples in the level of the PETM intervals where benthic foraminifera assemblages, although scarce, show a change from typical Late Cretaceous taxa like *Aragonia velascoensis and Aragonia ouzzanensis,* to PETM opportunistic taxa such as *Bulimina* sp., *Tappanina* sp. *and Quadrimorphina* sp.. This may be interpreted as a drop in the depth of the CCD. It correlates to the onset of the PETM as identified with nannofossils and carbon isotope correlates to the CIE and the BFE onset at 69.1 m in the section.

A negative excursion in δ13C values in the study section, known as the Carbon Isotope Excursion (CIE), coincides with the PETM in the Paryab section. The carbon isotope values (δ13C) fall from 1.5 to -0.2 per mil depicting the initial rapid negative carbon isotope excursion that is typical of continuous PETM sections.

Work in Progress

At the University of Massachusetts Amherst, we worked mostly on the specialized sample preparation for foraminifera extraction, including the Freeze dryer method. However, counting of the processed samples in more detail is still in progress, as the lab processing needed much time.

At the University of California Santa Cruz, we discussed various aspects of the project on the P-E boundary section in the Zagros. Isotopes were discussed in detail and the isotope interpretation was enhanced with focus on benthic foraminifera. Yet, isotope measurements of individual foraminifera could not be accomplished during the short visit time and had to be postponed for future lab work, also depending on extra financing. In the following, more time is needed to interpret the data in detail, which is now done at the home university, University of Vienna, to finish the PhD project and to write a publication, accordingly.

Future quantitative work on the samples will identify various proxy parameter and test the applicability of the BFOI to the section.

Discussion

The benthic foraminiferal extinction event (BEE or BFE, Thomas, 2003; Aubry et al., 2007) is known from many deep sea sections, both from bathyal and abyssal depths. According to Thomas (2003), Paleocene deep water habitats were populated by two benthic foraminiferal assemblages: (1) the *Nuttallides*-dominated assemblage group from predominantly abyssal depths, and (2) the bathyal assemblage of predominantly relict Late Cretaceous species characterized by *Stensioeina beccariiformis*. During the late Paleocene a gradual expansion of the bathymetric range from abyssal to middle bathyal depths of the *Nuttallides*-dominated assemblage at the expense of the

Stensioeina beccariiformis-dominated assemblage resulted in the replacement of the latter biofacies by the former and the abrupt extinction of over 50% of the Paleocene deep-water foraminiferal taxa. This extinction event-the BFE or BEE-was the most dramatic event in the evolution of deep water benthic foraminifera since the mid-Cretaceous (Gradstein et al., 2012). Among deep water taxa that became extinct are *Stensioeina beccariiformis, Angulogavelinella avnimelechi, Coryphostoma midwayensis, Aragonia velascoensis, A. ouzzanensis*, *Gavelinella hyphalus, G. rubiginosus (=G. danica), G. velascoensis, Neoflabellina jarvis and N. semireticulata, Neoeponides hillebrandti, Osangularia velascoensis,* and *Pullenia coryelli*.

Various processes abd causes have been discussed for the BEE, and a combination of factors has been concluded like elevated water temperatures, greater acidity and corrosivity of sea water, lower dissolved oxygen levels and a decrease in food supply (see Thomas, 2003, for a detailed review). Over the following 200.000 years, surviving species were gradually joined by newly evolved taxa that repopulated the ocean. Pre-PETM benthic foraminiferal fauna were remarkably uniform across a wide depth range, whereas the post-extinction fauna was diverse and showed depth-related distribution, most likely reflecting increase depth-related variations in physical/chemical properties of sea water (Thomas, 1998; Aubry et al., 2007).

In neritic to upper bathyal environments (the so-called Midway benthic foraminiferal fauna), the extinction of benthic foraminifera is also evident but less pronounced. *Angulogavelinella avnimelechi, Tritaxia midwayensis, Anomalinoides praeacutus* and *Cibicidoides succedens,* were eliminated from this habitat (Thomas et al., 1997; Aubry et al., 2007).

According to Kaiho et al. (2006) the percentage of “oxic” benthic foraminifera declines suddenly and significant below 0.1% at the BEE horizon (BEE) in deep sea sections such as in the tropical Pacific. This can be explained by the fact that if bottom waters are oxic, suboxic and disoxic

forms are still present, but primarily living several centimeters below the sediment/water interface as infauna. This explains why the percentages of the suboxic and disoxic indicators do not change in the lower portion of the PETM. However, in the upper portion of the PETM the ratio of suboxic/disoxic indicators increased from to about 1, coincident with the environmental recovery, indicating partial recovery of dissolved oxygen. During the interval when oxic species were absent, suboxic forms probably changed habitat and became more epifaunal, and thus more sensitive to bottom water oxygen conditions (Kaiho, 1994). As a consequence, the suboxic % or ratio of suboxic/disoxic (similar to BFOI) becomes a sensitive indicator of dissolved oxygen levels when oxic species were absent. In the Pacific Ocean sites, the gradually increasing BFOI values from −35 to −25 following the BEE reflect a gradual increase in ratio of suboxic / disoxic indicators. The fluctuations in BFOI values, oxic indicator (%), and suboxic indicator (%) in the absence of oxic indicators mainly reflects first-order changes of global deep-ocean ventilation and stagnation. A significant decrease in dissolved oxygen levels coincides with the BEE. The BFOI values imply a shift from low oxic (1.2–2.0 mL/L O2) to suboxic (0.3–1.2 mL/L O2) coeval with the onset of the PETM. A gradual rise in BFOI following the BEE indicates that dissolved oxygen levels increased slightly, but remained within suboxic conditions (Kaiho et al., 2007). The evolution of foraminifera at Parhab may show a similar succession, thus giving way to speculations on decreased oxygen levels at the PETM interval.

Conclusions

The Paryab section, NW Iran, records a continuous pelagic-hemipelagic sedimentation during the Paleogene within the Neo-Tethys. The section of the Padbeh Formation sheds light on late Paleocene to early Eocene stratigraphy. Nannofossil biostratigraphy constrains the studied section

to the standard nannofossil zones CNP8 to CNE8 (NP6 to NP14), indicating Selandian, Thentian, Ypresian to basal Lutetian ages. The Paleocene-Eocene Thermal Maximum (PETM) interval was identified by a significant negative carbon isotope excursion of c. 2‰. An age-depth plot using ages for nannofossil zones indicates continuous deposition, with varying sediment accumulation rates from 68 mm/ka in the lowermost part of the section to 6 mm/ka around the PETM interval.

Foraminiferal assemblages are characterized by a predominance of planktonic foraminifera, benthic foraminifera count less than 10% of the assemblages. Detailed foraminifera evaluation is still in progress. First results indicate a (Tethyan) planktonic foraminifera zonation around the PETM interval. The Benthic Foraminifera Extinction Event was identified in the PETM interval where benthic foraminifera assemblages, although scarce, show a change from typical Late Cretaceous taxa to opportunistic taxa. Shallowing of the CCD may be present. Future work will indicate more specific paleoceanographic changes regarding proxies like BFOI on the oxidation state during the PETM.

Acknowledgements

I thank the Marshall Plan Foundation and the University of Vienna authorities, namely Mr. Maximilian Kudler, for the fellowship stipend and thank my Marshall-Plan mentors Mark Leckie and James Zachos for hosting and supervising my work done in the USA. I thank UNESCO IGCP 609 *Climate-environmental deteriorations during greenhouse phases: Causes and consequences of short-term Cretaceous sea-level changes*, and the Austrian Academy of Sciences, International Research Programs, for financial support of the PhD project and the work done at the University of Vienna. The Department of Geodynamics and Sedimentology of the University of Vienna, and especially Sabine Hruby-Nichtenberger and Maria Meszar (all University of Vienna) are thanked for help in sample preparation and lab analyses.

References

Agnini, C., Fornaciari, E., Raffi, I., Catanzariti, R., Pälike, H., Backman, J., Rio, D., 2014. Biozonation and biochronology of Paleogene calcareous nannofossils from low and middle latitudes. Newsl. Stratigr. 47, 131–181.

Alegret, L., Ortiz, N., Molina, E., 2009a. Extinction and recovery of benthic foraminifera across the Paleocene-Eocene Thermal Maximum at the Alamedilla section (Southern Spain), Palaeogeogr. Palaeocl. Palaeoecol., 279, 186–200.

Alegret, L., Ortiz, S., Arenillas, I., Molina, E., 2010. What happens when the ocean is overheated? The foraminiferal response across the Paleocene-Eocene Thermal Maximum at the Alamedilla section (Spain), Geol. Soc. Am. Bull., 122, 1616–1624.

Alegret, L., Ortiz, S., Orue-Extebarria, X., Bernaola, G., Baceta, J.I., Monechi, S., Apellaniz, E., Pujalte, V., 2009b. The Paleocene-Eocene Thermal Maximum: New data on microfossil turnover at the Zumaia section, Spain, Palaios, 24, 318–328.

Alve, E., Goldstein, S.T., 2003. Propagule transport as a key method of dispersal in benthic foraminifera (Protists), Limnol. Oceanogr., 48, 2163–2170.

Aubry, M.-P., Ouda, K., Dupuis, C. et al., 2007. Global Standard Stratotype-section and Point (GSSP) for the base of the Eocene Series in the Dababiya section (Egypt). Episodes, 30, 271– 286

Azami, S.H., Wolfgring, E., Wagreich, M., Gharaie, M.H.M., 2018. Paleocene-Eocene Calcareous Nannofossil Biostratigraphy and Cyclostratigraphy From the Neo-Tethys, Pabdeh Formation of the Zagros Basin (Iran). Stratigraphy & Timescales, Volume 3, 357-383 (Elsevier). https://doi.org/10.1016/bs.sats.2018.08.006.

Barbarian, M., King, G.C.P., 1981. Towards a paleogeography and tectonic of Iran. Canadian J. Earth Sci, 18, 210–265.

Berger, W.H., Bonneau, M.C., Parker, F.L., 1982. Foraminifera on the deep-sea floor: Lysocline and dissolution rate. Oceanol. Acta, 5(2):249–258.

Berggren, W.A., Aubert, J., 1975. Paleocene benthonic foraminiferal biostratigraphy, paleobiogeography and paleoecology of Atlantic-Tethyan regions: Midway-type fauna. Palaeogeography, Palaeoclimatology, Palaeoecology, 18, 73-192.

Bowen, G.J., Zachos, J.C., 2010. Rapid carbon sequestration at the termination of the Palaeocene–Eocene Thermal Maximum. Nature Geosci., 3, 866–869.

Bown, P.R. (Ed.). Calcareous Nannofossil Biostratigraphy. British Micropalaeontological Soc. Publ. Ser., Chapman and Hall, London.

Bralower, T.J., 2002. Evidence of surface water oligotrophy during the Paleocene –Eocene thermal maximum: Nannofossil assemblage data from Ocean Drilling Program Site 690, Maud Rise, Weddell Sea. Paleoceanography, 17 (2) PA1023.

Broecker, W.S., Clark, E., 1999. CaCO3 size distribution: a paleocarbonateion proxy? Paleoceanography, 14(5):596–604.

Cetean, C.G., Balc, R., Kaminski, M.A., Filipescu, S., 2011. Integrated biostratigraphy and palaeoenvironments of an upper Santonian-upper Campanian successionfrom the southern part of the Eastern Carpathians, Romania. Cretac. Res. 32, 575-590.

Corliss, B.H. Chen, C., 1988. Morphotype patterns of Norwegian Sea deep-sea benthic foraminifera and ecological implications, Geology, 16, 716–719.

Corliss, B.H., 1985. Microhabitats of benthic foraminifera within deep-sea sediments, Nature, 314, 435–438, 1985.

DeConto, R.M., Galeotti, S., Pagani, M., Tracy, D., Schaefer, K., Zhang, T., Pollard, D., Beerling, D.J., 2012. Past extreme warming events linked to massive carbon release from thawing permafrost. Nature, 484, 87-91.

Dickens, G.R., Castillo, M.M., Walker, J.C.G., 1997. A blast of gas in the latest Paleocene: Simulating first-order effects of massive dissociation of oceanic methane hydrate. Geology, 25 (3), 259–262.

Dunkley Jones, T., Lunt, D.J., Schmidt, D.N., Ridgwell, A., Sluijs, A., Valdes, P.J., Maslin, M., 2013. Climate model and proxy data constraints on ocean warming across the Paleocene–Eocene Thermal Maximum. Earth Sci. Rev., 125, 123–145.

Frenzel, P., 2000. Die benthischen Foraminiferen der Rügener Schreibkreide (unter-Maastricht, NE Deutchland). CPress, Dresden.

Friedrich, O., 2010. Benthic foraminifera and their role to decipher paleoenviron-ment during mid-Cretaceous Oceanic Anoxic Events e the “anoxic benthic foraminifera” paradox. Rev. micropaleontology, 53, 175-192.

Friedrich, O., Erbacher, J., Mutterlose, J., 2006. Paleoenvironmental changes across the cenomanian/turonian boundary event (oceanic anoxic event 2) as indicated by benthic foraminifera from the demerara Rise (ODP Leg 207). Rev. Micropaleontologie, 49, 121-139.

Friedrich, O., Nishi, H., Pross, J., Schmiedl, G., Hemleben, C., 2005. Millennial to centennial-scale interruptions of the Oceanic Anoxic Event 1b (Early Albian, mid-Cretaceous) inferred from benthic foraminiferal repopulation events. Palaios, 20, 64-77.

Gibson, T.G., Bybell, L.M., Owens, J.P., 1993. Latest Paleocene lithologic and biotic events in neritic deposits of southwestern New Jersey. Paleoceanography, 8, 495–514.

Gingerich, P.D., 2003. Mammalian response to climate change at the Paleocene-Eocene boundary: Polecat Bench record in the northern Bighorn Basin, Wyoming. In: Geol. S. Am. S. (Eds.), Wing, S. L.,

Gingerich, P. D., Schmitz, B., and Thomas, E., Boulder, Colorado, The Geological Society of America, 369, 463–478.

Giusberti, L., Boscolo Galazzo, F., Thomas, E., 2016. Variability in climate and productivity during the Paleocene–Eocene Thermal Maximum in the western Tethys (Forada section). Climate of the Past. 12, 213–240.

Gradstein, F.M., Ogg, J.G., Schmitz, M.D., Ogg, G.M., 2012 (Eds.). The Geological Time Scale 2012. Amsterdam, Elsevier.

Hancock, H.J.L. Dickens, G.R., 2005. Carbonate dissolution episodes in Paleocene and Eocene sediment, Shatsky Rise, west-central Pacific. In: Bralower, T.J., Premoli Silva, I., Malone, M.J. (Eds.), Proceedings of the Ocean Drilling Program, Scientific Results, 198.

Hayward, B.W., Kawagata, S., Sabaa, A.T., Grenfell, H.R., van Kerckhoven, L., Johnson, K., Thomas, E., 2012. The Last Global Extinction (Mid-Pleistocene) of Deep-Sea Benthic Foraminifera (Chrysalogoniidae, Ellipsoidinidae, Glandulonodosariidae, Plectofrondiculariidae, Pleurostomellidae, Stilostomellidae), their Late Cretaceous-Cenozoic History and Taxonomy, Cushman Foundation for Foraminiferal Research Special Publication, 43, Allen Press, Lawrence, USA, 408 pp.

Higgins, J.A., Schrag, D.P., 2006. Beyond methane: Towards a theory for the Paleocene–Eocene Thermal Maximum. Earth Planet. Sci. Lett., 245 (3–4), 523–537.

Hönish et al., 2012. Science 335, 1058-1063.

Jaramillo, C.A., Ochoa, D., Contreras, L., Pagani, M., Carvajal Ortiz, H., Pratt, L.M., Krishnan, S., Cardona, A., Romero, M., Quiroz, L., Rodriguez, G., Rueda, M.J., De la Parra, F., Morón, S., Green, W., Bayona, G., Montes, C., Quintero, O., Ramirez, R., Mora, G., Schouten, S., Bermudez, H., Navarrete, R., Parra, F., Alvarán, M., Osorno, J., Crowley, J.L., Valencia, V., Vervoort, J.,

2010 Effects of rapid global warming at the Paleocene-Eocene boundary on Neotropical vegetation, Science, 330, 957–961.

Jones, R.W., Charnock, M.A., 1985. “Morphogroups” of agglutinated foraminifera. Their life positions and feeding habits and potential applicability in (paleo) ecological studies, Revue de Paléobiologie, 4, 311–320.

Jorissen, F.J., de Stigter, H.C., Widmark, J.G.V., 1995. A conceptual model explaining benthic foraminiferal microhabitats. Mar. Micropaleontol, 26, 3-15.

Kaiho, K., 1994. Benthic foraminiferal dissolved-oxygen index and dissolved-oxygen levels in the modern ocean. Geology, 22, 719–722.

Kaiho, K., Takeda, K., Petrizzo, M.R., Zachos, J.C., 2006. Anomalous shifts in tropical Pacific planktonic and benthic foraminiferal test size during the Paleocene–Eocene thermal maximum. Palaeogeography, Palaeoclimatology, Palaeoecology, 237, 456-464.

Kaminski, M.A., Gradstein, F.M., 2005. Atlas of Paleogene Cosmopolitan Deep-water Agglutinated Foraminifera. Grzybowski Foundation Special Publication, Poland.

Kelly, D.C., Bralower, T.J., Zachos, J.C., Premoli-Silva, I., Thomas, E., 1996. Rapid diversification of planktonic foraminifera in the tropical Pacific (ODP Site 865) during the late Paleocene thermal maximum. Geology, 24 (5), 423–426.

Kelly, D.C., Zachos, J.C., Bralower, T.J., and Schellenberg, S.A., 2005. Enhanced terrestrial weathering/runoff and surface ocean carbonate production during the recovery stages of the Paleocene- Eocene thermal maximum. Paleoceanogr., 20, 1–11.

Kennett, J.P., Stott, L.D., 1991. Abrupt deep-sea warming, palaeoceanographic changes and benthic extinctions at the end of the Palaeocene. Nature, 353 (6341), 225-229.

Kent, D.V., Cramer, B.S., Lanci, L., Wang, D., Wright, J.D., Van der Voo, R., 2003. A case for a comet impact trigger for the Paleocene/Eocene thermal maximum and carbon isotope excursion. Earth Planet. Sci. Lett. 211 (1–2), 13–26.

Koutsoukos, E.A.M., Hart, M.B., 1990, Cretaceous foraminiferal morphogroup distribution patterns, paleocommunities and trophic structures: A case study from the Sergipe Basin, Brazil: Royal Society of Edinburgh, Transactions, Earth Sciences, 81, 221–246.

Koutsoukos, E.A.M., Leary, P.N., Hart, M.B., 1990. Latest Cenomanian-earliest Turonian low-oxygen tolerant benthonic foraminifera: A case-study from the sergipe basin (N.E. Brazil) and the western Anglo-Paris basin (southern England). Palaeogeogr. Palaeoclimatol. Palaeoecol., 77, 145-177.

Le, J., Shackleton, N.J., 1992. Carbonate dissolution fluctuations in the western equatorial Pacific during the late Quaternary. Paleoceanography, 7(1):21–42.

Leckie, R.M., Olson, H., 2003. Foraminifera as proxies of sea-level change on siliciclastic margins. In: Olson, H.C., Leckie, R.M. (Eds.), Micropaleontologic Proxies of Sea-Level Change and Stratigraphic Discontinuities. Tulsa, SEPM (Society of Sedimentary Geology), Special Publication 75, 5-19.

Malmgren, B.A., 1987. Differential dissolution of Upper Cretaceous planktonic foraminifera from a temperate region of the South Atlantic Ocean. Mar. Micropaleontol., 11(4):251–271.

Mancin, N., Hayward, B.W., Trattenero, I., Cobianchi, M., Lupi, C., 2013. Can the morphology of deep-sea benthic foraminifera reveal what caused their extinction during the mid-Pleistocene Climate Transition?, Mar. Micropaleont., 104, 53–70.

Martini, E., 1971. Standard Tertiary and Quaternary calcareous nannoplankton zonation. In: Farinacci, A. (Ed.), Proceedings 2nd International Conference Planktonic Microfossils Roma, Rome 2, 739–785.

McInerney, F.A., Wing, S. L., 2011.The Paleocene–Eocene Thermal Maximum: a perturbation of carbon cycle, climate, and biosphere with implications for the future. Annu. Rev. Earth P lanet. Sci., 39, 489–516.

Pagani, M., Caldeira, K., Archer, D., Zachos, J.C, 2006. An ancient carbon mystery. Science, 314, 1556–1557.

Saura, E., Vergés, J., Homke, S. et al., 2011. Basin architecture and growth folding of the NW Zagros early foreland basin during the Late Cretaceous and early Tertiary. J. Geol. Soc. London 168, 235–250.

Schlanger, S.O., Douglas, R.G., 1973. Porosity and textural changes related to the ooze-chalk-limestone transition. Eur. Geophys. Soc. Meet. Abstr., 1:92.

Speijer, R.P., Scheibner, C., Stassen, P., Morsi, A.-M., 2012. Response of marine ecosystems to deep-time global warming: A synthesis of biotic patterns across the Paleocene-Eocene thermal maximum (PETM), Austr. J. Earth Sci., 105, 6–16.

Stassen, P., Thomas, E., Speijer, R.P., 2015. Paleocene-Eocene Thermal Maximum environmental change in the New Jersey Coastal Plain: benthic foraminiferal biotic events, Mar. Micropaleont., 115, 1–23.

Şengör, A.M.C., 1990. A new model for late Paleozoic- Mesozoic tectonic evolution of Iran and implications for Oman. in Robertson, A.H.F., Searle, M.P., Ries, A.C. (Eds.). The Geology and Tectonics of the Oman Region. Geol. Soc. Spec. Publ. 49, 797–783.

Svensen, H., Planke, S., Malthe-Sorenssen, A., Jamtveit, B., Myklebust, R., Eidem, T.R., Rey, S.S., 2004. Release of methane from a volcanic basin as a mechanism for initial Eocene global warming. Nature, 429 (6991), 542–545.

Thomas, E., 1989. Development of Cenozoic deep-sea benthic foraminiferal faunas in Antarctic waters. Geol. Soc. Lond., Spec. Publ., 47 (1), 283–296.

Thomas, E., 1998. Biogeography of the Late Paleocene benthic foraminiferal extinction. In: Aubry, M.-P., Lucas, S.H., Berggren, W.A. (Eds.), Late Paleocene–Early Eocene Climatic and Biotic Events in the Marine and Terrestrial Records. Columbia University Press, New York, pp. 214–243.

Thomas, E., 2007. Cenozoic mass extinctions in the deep sea: What perturbs the largesthabitat on Earth? In: Monechi, S., Coccioni, R., Rampino, M.R. (Eds.), Large Ecosystem Perturbations: Causes and Consequences. Geological Society of America, Special Paper, 424, pp. 1–13.

Thomas, E., Shackleton, N.J., 1996. The Paleocene–Eocene foraminiferal extinction and stable isotope anomalies. In: Knox, R.W.O.B., Corfield, R.M., Dunay, R.E. (Eds.), Correlation of the Early Paleogene in Northwest Europe. Geological Society Special Publication, 101, pp. 401–441.

Thomas, E., Shackleton, N.J., 1996. The Paleocene–Eocene foraminiferal extinction and stable isotope anomalies. In: Knox, R.W.O.B., Corfield, R.M., Dunay, R.E. (Eds.), Correlation of the Early Paleogene in Northwest Europe. Geological Society Special Publication, 101, pp. 401–441.

Thomas, E., 2003. Extinction and food at the seafloor: A high-resolution benthic foraminiferal record across the Initial Eocene Thermal Maximum, Southern Ocean Site 690. In: Wing, S.L., Gingerich, P.D., Schmitz, B., Thomas, E. (Eds.), Causes and Consequences of Globally Warm Climates in the Early Paleogene. Geol. S. Am. S., Boulder, Colorado, The Geological Society of America, 369, 319–332.

Thunell, R.C., 1976. Optimum indices of calcium carbonate dissolution in deep-sea sediments. Geology, 4(9):525–528.

Tjalsma, R.C., Lohmann, G.P., 1983. Paleocene–Eocene bathyal and abyssal benthic foraminifera from the Atlantic Ocean. Micropaleontology, Special Publication, 4, 1–90.

Van der Zwaan, G.J., Duijnstee, I.A.P., den Dulk , M., Ernst, S.R., Jannink , N.T., Kouwenhoven, T.J., 1999. Benthic foraminifers: proxies or problems? A review of paleoecological concepts. Earth-Science Rev., 46, 213-236.

Van Hinsbergen, D.J.J., Kouwenhoven, T.J., Van der Zwaan, G.J., 2005. Paleobathymetry in the backstripping procedure: Correction of oxygenation effects on depth estimates. Palaeogeogr. Palaeoclimatol. Palaeoceology., 21, 245-265.

Waters, C.N., Zalasiewicz, J., Summerhayes, C. et al., 2016. The Anthropocene is functionally and stratigraphically distinct from the Holocene. Science 351, 6269, aad2622.

Westerhold, T., Röhl, U., Frederichs, T., Bohaty, S. M., and Zachos, J. C., 2015. Astronomical calibration of the geological timescale: closing the middle Eocene gap. Clim. Past, 11, 1181–1195.

Westerhold, T., Röhl, U., Friedrichs, T., Agnini, C., Raffi, I., Zachos, J.C., Wilkens, R.H., 2017. Astronomical calibration of the Ypresian timescale: implications for seafloor spreading rates and the chaotic behavior of the solar system. Clim. Past, 13, 1129–1152.

Westerhold, T., Röhl, U., Laskar, J., 2012. Time scale controversy: Accurate orbital calibration of the early Paleogene. Geochem., Geophys., Geosyst., 13/6.

Williams, D.F., Healy-Williams, N., Leschak, P., 1985. Dissolution and water-mass patterns in the Southeast Indian Ocean. Part I. Evidence from Recent to late Holocene foraminiferal assemblages. Geol. Soc. Am. Bull., 96(2):176–189.

Wing, S.L., Harrington, G.J., Smith, F.A., Bloch, J.I., Boyer, D.M., Freeman, K.H., 2005. Transient floral change and rapid global warming at the Paleocene-Eocene boundary, Science, 310, 993–996.

Zachos, J.C., Dickens, G.R., Zeebe, R.E., 2008. An early Cenozoic perspective on greenhouse warming and carbon-cycle dynamics. Nature, 451 (7176), 279–283.

Zachos, J.C., Pagani, M., Sloan, L., Thomas, E., Billups, K., 2001. Trends, rhythms, and aberrations in global climate 65 Ma to present. Science, 292, 686-693.

Zeebe, R.E., Dickens, G.R., Ridgwell, A., Sluijs, A., Thomas, E., 2014. Onset of carbon isotope excursion at the Paleocene-Eocene Thermal Maximum took millennia, not 13 years (Comment), P. Natl. Acad. Sci. USA, 111, E1062–E1063.

Zachos, J.C., Wara, M. W., Bohaty, S., Delaney, M. L., Petrizzo, M.R., Brill, A., Bralower, T.J., Premoli-Silva, I., 2003. A transient rise in tropical sea surface temperature during the Paleocene– Eocene thermal maximum. Science 302, 1551–1554.

Zachos, J.C., Röhl, U., Schellenberg et al., 2005. Rapid acidification of the ocean during the Paleocene–Eocene thermal maximum. Science 308, 1611–1615.

Seyed Hamidreza Azam, Vienna, August 2019